Endocytosis is required for E-cadherin redistribution at mature *adherens* junctions

Simon de Beco[a,b], Charles Gueudry[a,b], François Amblard[a,b,1,2], and Sylvie Coscoy[a,b,1,2]

[a]Centre de Recherche, Institut Curie, F-75248 Paris, France; and [b]Centre National de la Recherche Scientifique, Unité Mixte de Recherche 168, F-7524 Paris, France

Edited by Masatoshi Takeichi, RIKEN, Kobe, Japan, and approved March 10, 2009 (received for review November 14, 2008)

E-cadherin plays a key role at *adherens* junctions between epithelial cells, but the mechanisms controlling its assembly, maintenance, and dissociation from junctions remain poorly understood. In particular, it is not known to what extent the number of E-cadherins engaged at junctions is regulated by endocytosis, or by dissociation of adhesive bonds and redistribution within the membrane from a pool of diffusive cadherins. To determine whether cadherin levels at mature junctions are regulated by endocytosis or dissociation and membrane diffusion, the dynamics of E-cadherin were quantitatively analyzed by a new approach combining 2-photon fluorescence recovery after photobleaching (FRAP) and fast 3D wide-field fluorescence microscopy. Image analysis of fluorescence recovery indicates that most E-cadherin did not diffuse in the membrane along mature junctions, but followed a first order turn-over process that was rate-limited by endocytosis. In confluent cultures of MCF7 or MDCK cells, stably expressed EGFP-E-cadherin was rapidly recycled with spatially uniform kinetics (50 s in MCF7 and 4 min in MDCK). In addition, when endocytosis was pharmacologically blocked by dynasore or MiTMAB, no fluorescence recovery was observed, suggesting that no endocytosis-independent membrane redistribution was occurring. Our data show that membrane redistribution of E-cadherin molecules engaged in mature junctions requires endocytosis and subsequent exocytosis, and lead to the notion that E-cadherins engaged at junctions do not directly revert to free membrane diffusion. Our results point to the possibility that a direct mechanical coupling between endocytosis efficiency and cadherin-mediated forces at junctions could help to regulate intercellular adhesion and locally stabilize epithelia.

diffusion | fluorescence recovery after photobleaching

E-cadherin is a calcium-dependent adhesion receptor present in *adherens* junctions of epithelial cells that plays an important role during embryonic development and in establishing cell–cell adhesions in mature epithelia (1, 2). It is also involved in cell polarization, compaction, and wound healing mechanisms. Its down-regulation is an important step during the epithelium-to-mesenchyme transition and the appearance of invasive phenotypes (3). E-cadherin is a transmembrane protein and its intracellular domain interacts with multiple components including β-, α-, and γ-catenins, leading to indirect interactions with the contractile actin-myosin cortex (1, 4). The extracellular domain, with 5 tandem repeats, is engaged in homophilic adhesive interactions.

Through the extracellular domains, cadherins can interact in *trans* (engaged state) with cadherins on neighboring cells or in *cis* with cadherins laterally within the same membrane (5). Although several studies have been devoted to quantifying adhesion forces and energies between cadherin molecules or cadherin-bearing cells, the extent of the force and energy of isolated *trans* bonds remains controversial, and the role of *cis*-bonds is poorly understood. Most experiments suggest that cadherins form low-affinity interactions (1), but there is also biochemical evidence for stable interactions (6, 7). The differential membrane organization of cadherins through *cis*-dimerization and *cis*-trans cluster formation may likely account for many unsolved puzzles, such as the discrepancy between low molecular affinities and strong adhesion.

E-cadherin drives the formation of intercellular contacts through several processes (exocytosis, diffusion, clustering) (8), and its dynamic behavior is involved in the maintenance and adaptation of the mature junction. This article addresses the behavior of E-cadherin in "mature junctions," defined as the stationary state achieved $\approx$24 h after the onset of cell–cell contact where E-cadherin levels and junctional distribution are stabilized. In mature junctions, E-cadherin remains highly dynamic, as evidenced by lifetimes of a few minutes for high-affinity adhesive *trans* dimers in A431 cells (9). Indeed, the maintenance of stable multicellular assemblies requires that adhesive forces and internal contractile tensions be finely balanced and able to compensate for variations of force applied on both sides of the junction. Highly dynamic cadherin distributions could help cells to quickly respond to internal and external morphogenetic stimuli by modulating local cadherin numbers, and might hence be necessary to maintain mechanically stable epithelia.

The mechanisms by which cadherin concentration is controlled at mature junctions are under debate and 2 distinct hypothesis are considered. First, the plasma membrane could contain a large pool of freely diffusive individual cadherins acting as a "reservoir" for the formation of low-affinity *trans* bonds organized into clusters. Reversible dissociation from those clusters could yield freely diffusing individual cadherins able to directly engage into adhesion again (10). The second model hypothesizes that, once inserted into the plasma membrane, E-cadherins could rapidly form high-affinity *trans* contacts that could be disrupted mainly by endocytosis (11). E-cadherin endocytosis has been widely described (12). It occurs via different internalization routes depending on cell types or physiological situations, and cadherin is recycled in a highly controlled way.

To better understand how E-cadherin concentration is regulated at mature junctions, a quantitative investigation of membrane diffusion and turnover is needed, and a clarification of the role of endocytosis versus direct reversion from adhesive binding back to diffusing freely in the membrane. Single-particle tracking and fluorescence recovery after photobleaching (FRAP) experiments have suggested the existence of a large pool of membrane diffusive E-cadherins, but those experiments were generally not performed in mature junctions (8, 10, 13, 14). Additionally,

Author contributions: S.d.B., F.A., and S.C. designed research; S.d.B. performed research; C.G. contributed new reagents/analytic tools; S.d.B., F.A., and S.C. analyzed data; and S.d.B., F.A., and S.C. wrote the paper.

The authors declare no conflict of interest.

This article is a PNAS Direct Submission.

[1]S.C. and F.A contributed equally to this work.

[2]To whom correspondence may be addressed. E-mail: francois.amblard@curie.fr or sylvie.coscoy@curie.fr.

This article contains supporting information online at www.pnas.org/cgi/content/full/0811253106/DCSupplemental.

www.pnas.org/cgi/doi/10.1073/pnas.0811253106

biochemical analyses on mature junctions, not aimed at measuring the contribution of diffusion, have suggested that endocytosis only concerned a restricted pool of cadherin molecules (15).

In the present work, we have quantitatively studied the respective roles of membrane diffusion and endocytosis in the dynamics of E-cadherin in mature junctions. A new approach combining 2-photon FRAP and fast 3D fluorescence microscopy has enabled detailed image analysis of fluorescence relaxation in 3D space. Two-photon FRAP allows photobleaching to be restricted within the focal volume ($\approx 1\ \mu m^3$) (16, 17). Because the junction plane in standard cell cultures is parallel to the optical axis, 2-photon FRAP is necessary to restrict photobleaching at the junction, and limit out-of-focus fluorescence depletion in the cytoplasm. In addition, the analysis of the fluorescent recovery process from series of 3D image stacks in a full spatial extent around a photobleached volume is used here. Our results with 2 epithelial cell lines show that the membrane organization dynamics at steady-state in mature junctions is mainly, if not only, accounted for by endocytosis and subsequent exocytosis in a first-order rate-limited manner. We also find that this behavior applies to all E-cadherins at a junction, and not only to a minor pool as suggested (15).

Results

Principles of FRAP Experiments. E-cadherin local dynamics were studied in mature junctions, that is, junctions engaged in adhesion for many hours, in which cadherin expression level is stable. We determined the respective influences of diffusion or vesicular trafficking (endocytosis/exocytosis) in regulating local E-cadherin levels. Two epithelial cell lines were studied, MDCK cells derived from canine proximal kidney and MCF7 cells derived from a human breast cancer. These cells may have different adhesive properties as a less rigorous EDTA treatment is needed to dissociate MCF7 cell–cell contacts. In vitro, these cell lines both form epithelial layers, but MCF7 cells are able to generate tumors in vivo whereas MDCK cells are not. After stable transfection with E-cadherin-GFP (8), E-cadherin dynamics were studied by 2-photon FRAP combined with 3D widefield fluorescence microscopy, which allowed the recovery process to be analyzed from series of image stacks in the entire 3D region surrounding the photobleached volume. For the interpretation of FRAP data, we considered the following possibilities for mediation of E-cadherin dynamics: membrane diffusion (Fig. 1*A 1*), vesicle-mediated endocytosis (Fig. 1*A 2*), and exchange between mobile and immobile pools at the plasma membrane (Fig. 1*A 3*).

The shape of the recovery curve allowed us to distinguish diffusive from first-order reaction-limited exchange processes. The latter may correspond to exchange by endocytosis/exocytosis or exchange at the membrane between a mobile (diffusive) and an immobile (engaged) pool. In the case of reaction-limited exchange, the recovery curve only depends on the off-rate, and yields an estimate of the residence time in the membrane (16–18). A more general scenario would be to couple 3 states (diffusion, immobile, cytosolic), but that level of complexity was not necessary to account for our observations (see SI).

Because fluorescence recovery is accessible through image series in our set-up, more complex scenarios could be evaluated by analyzing how spatial fluorescence concentration profiles evolved with time (Fig. 1 *B–D*). As a simple example, the width of a zone containing photobleached molecules increase with time for diffusion (Fig. 1 *B* and *D*), but it remains constant in the case of first-order reaction-limited exchange (Fig. 1 *C* and *D*). In the latter case, the recovery kymograph corresponds to a spatial Gaussian distribution of constant width with an exponentially decaying amplitude

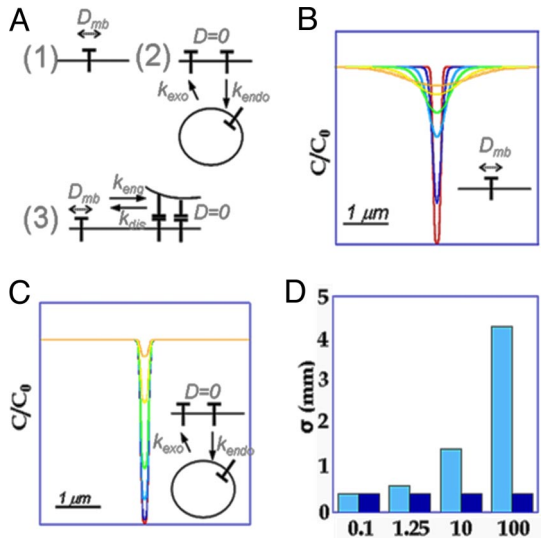

Fig. 1. Frame for FRAP data interpretation. (*A*) Different types of mobility are considered for membrane E-cadherin: membrane diffusion (*1*) or reaction-limited exchange with cytosolic vesicles via endocytosis (*2*) or between 2 membrane populations (*3*). (*B* and *C*) Fluorescence profile after photobleaching with $D_{mb} = 0.05\ \mu m^2 \cdot s^{-1}$ (*B*) or exchange with $k_{off} = 0.025\ s^{-1}$ (*C*), at $t = 0$ (red), $t = 1$ s (blue), $t = 6$ s (cyan), $t = 15$ s (green), $t = 45$ s (yellow), or $t = 100$ s (orange). Individual profiles were fitted to a Gaussian. (*D*) Evolution of σ as a function of time (cyan: diffusion, blue: exchange).

$$F(x,t) = 1 - \underbrace{a_0 e^{-t/T_{res}}}_{temporal}\ \underbrace{e^{-(x-x_0)^2/2\sigma^2}}_{spatial}$$

(a_0 amplitude). In this model, the recovery rate is the same in each point. Only the initial bleach amplitude ($1 - a_0 e^{-(x-x0)^2/2\sigma^2}$) varies along the axis.

E-Cadherin Dynamics in MDCK Junctions Reflects Reaction-Limited Exchange with a 240-s Residence Time. We first investigated E-cadherin dynamics in the mature junctions of MDCK cells (Fig. 2*A*). In *adherens* junctions of MDCK cells, E-cadherin is present as a 2.5-μm vertical stripe, with approximately uniform intensity (see SI). FRAP experiments targeted this stripe, with a *z*-resolution of 1.8 μm (NA = 1.25) that is similar to the vertical extension of E-cadherin localization. Fluorescence recovery along junctions was analyzed as a function of time (Fig. 2 *B* and *C*).

The photobleached profile fits well with a Gaussian profile that evolves in time with a constant width corresponding to the size of the photobleached region (0.5 μm) (Fig. 2*D*), strongly suggesting that the process is dominated by a reaction-dominant exchange, with only a minor contribution of diffusion at membrane. Indeed, an exponential function ($F(x = 0,t) = 1 - a_0 e^{-t/T_{res}}$) with a characteristic time T_{res} of 240 s (185–312 s) fits well to the recovery curve on the photobleached point over >3 decades of the time axis (Fig. 2*E*). In contrast, diffusion would have given a quite different recovery profile. Importantly, the long observation times (20 min) allowed by 3D videomicroscopy made it possible to correct for the movement of junctions and to follow the recovery to completion. At this time scale, the mobile fraction was 100%.

Although diffusion is not visible over long times, observations at shorter times showed the existence of a small ($\approx$5–10%) level of recovery that can only be explained by diffusion (Fig. 2*E Upper Left Inset*). Because the setting of an upper bound to the percentage of the fast membrane diffusive component is complicated on recovery curves due to the incomplete separation of

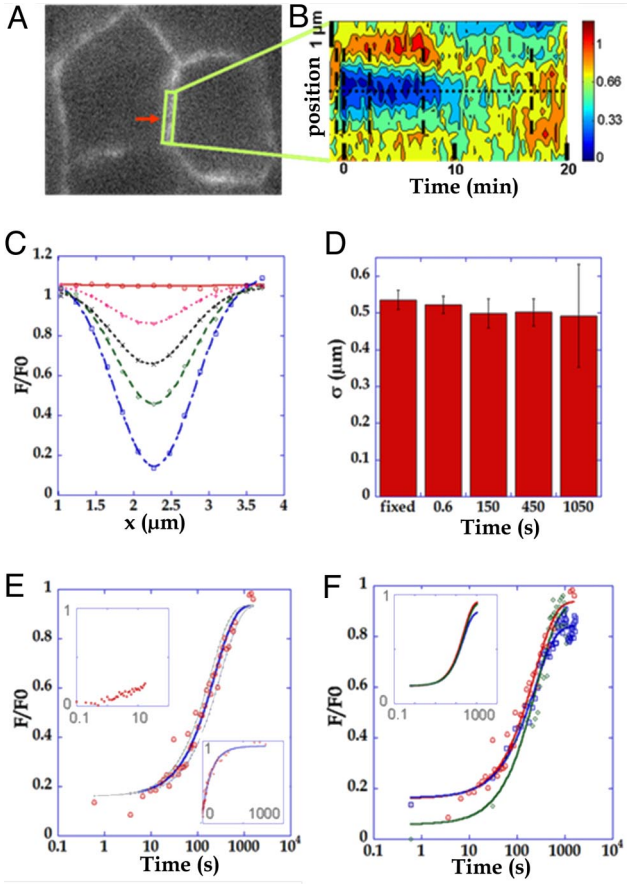

Fig. 2. Two-photon FRAP experiments at mature *adherens* junctions of MDCK-E-cadherin-GFP cells. (*A*) Two-photon FRAP was performed in a 1 μm-radius ellipsoid spot (red arrow) at *adherens* junctions in MDCK cells stably expressing E-cadherin-GFP. Fluorescence recovery was analyzed in the surrounding region (green frame). (*B*) A kymograph representing the intensity along the junction (*y* axis) as a function of time (*x* axis) is represented. (*C*) Profile analysis of the recovery. 16 fluorescence profile mean curves along the junction, before bleaching (red circle) and at 0.6 s (blue square), 150 s (green diamond), 450 s (black x), and 1,050 s (pink +) after photobleaching are shown. All postbleach curves are fitted by Gaussian models (dashed lines). (*D*) The width of the gaussians at different times after photobleaching are compared with the reference width after photobleaching in fixed cells. (*E*) The fluorescence recovery curve (red circle, $n = 45$) is well fit (blue line) by a first-order exchange model with $k_{off} = 0.0043\ s^{-1}$ (gray: $k_{off} = 0.0043 \pm 0.0011\ s^{-1}$). (*Upper Left Inset*) Shorter timescales ($\Delta t = 100$ ms, $n = 31$). (*Right Lower Inset*) Linear time axis representation. (*F*) Photobleaching spots of 0.5 ($n = 45$, red circle), 0.8 ($n = 20$, blue square) and 1.2 ($n = 20$, green diamond) μm width along the junction axis are well fitted by first-order exchange with similar coefficients of $k_{off} = 0.0043$, 0.0043 and 0.0039 s^{-1} respectively. (*Upper Left Inset*) The latter fitting curves were normalized so that the photobleaching depth is the same for all conditions.

time scales of short-time and long-time processes, this maximal percentage of diffusive component was calculated through the widening of the photobleached area during the time of fluorescence relaxation. If one assumes that the error bars on Gaussian width (Fig. 2*D*) increase with time because of an effective widening, the maximal percentage of a diffusive pool can be estimated at 5% of membrane cadherins (see SI). Hence a very minor diffusive component does exist and is either independent, or exchanges with the immobile pool with slow on-rates and in a quasi-irreversible way ($k_{eng} > 20k_{dis}$) (see SI).

To confirm that the process was largely dominated by first-order exchange, the size of the photobleached zone was increased to test whether the relaxation kinetics were dependent upon the size of the photobleached area. Upon photobleaching an enlarged region with 1, 3, or 5 adjacent points (0.5-, 0.8-, or 1.2-μm-long zones), similar recovery kinetics were seen, with very close k_{off} estimates (4.3 ± 1, 4.3 ± 1 and $3 \pm 0.8 \times 10^{-3}\cdot s^{-1}$, respectively) (Fig. 2*F*). Moreover, fluorescence recovery was studied in different points of the photobleached area, and k_{off} was the same independent of the position relative to the photobleached spot. This again shows that E-cadherin mobility is mostly due to a rate-limiting exchange and not to diffusion. Importantly, this exchange behavior observed in mature junctions contrasts with the membrane-diffusive behavior reported in the litterature in experimental situations without engagement (8, 10, 13). In agreement with the litterature, we found a diffusive behavior in our experiments aimed at producing "nonmature" (dissociating) junctions. After partial dissociation induced by EDTA, and in the presence of dynasore, a nonmature situation was observed, defined as the loss of contacts between cells and the reduction of E-cadherin levels at junctions. In contrast to the "mature" situation, a diffusive behavior was observed. The width σ^2 of the Gaussian profile increased linearly with time, consistent with an effective diffusion coefficient of 0.0025 $\mu m^2\cdot s^{-1}$ (see SI).

Inhibition of Endocytosis with Dynasore or MiTMAB Suppresses E-Cadherin Dynamics in MDCK Cells. To further study the role of endocytosis in the local turnover of cadherin, we specifically blocked endocytosis with dynasore, a potent inhibitor of dynamin-dependent endocytic pathways. Dynasore acts as a noncompetitive inhibitor of the GTPase activity of dynamin, with an IC50 of 15 μM. Previous studies established that dynasore does not affect dynamin-independent functions (19), and does not inhibit exocytosis at short timescales (20). We confirmed that dynasore treatment was effective by visualizing vesicle formation either using FM4–64 staining (all vesicles are positive). An almost near complete suppression of FM4–64 positive vesicles formation in dynasore-treated cells was observed (Fig. 3 *B–B″* vs. *A–A″* and Table 1). The total number of E-cadherin-GFP containing vesicles did not change upon dynasore treatment (Table 1); together with FRAP experiments shown below, this is in agreement with the steady-state hypothesis, i.e., conservation of the numbers of E-cadherin molecules both at membrane and in the cytosolic pool during treatment. However, the number of newly formed E-cadherin-GFP containing vesicles, as identified by the colocalization of green and red staining, was significantly reduced upon treatment with dynasore, and increased significantly faster in control conditions, but not with the drug (Table 1 and Fig. 3 *B–B″* vs. *A–A″*). Importantly, these experiments indicate that almost half of the E-cadherin molecules found in cytosolic vesicles have been taken up from the membrane within <3 min in normal conditions, in agreement with the fast cycling suggested by our FRAP experiments. The morphology of *adherens* junctions was preserved upon dynasore treatment (SI).

Interestingly, a 15-min incubation with 60 μM dynasore completely suppressed fluorescence recovery, as indicated by fluorescence recovery curves (Fig. 3*D*) and profile curves showing that the concentration profile did not evolve with time after photobleaching (Fig. 3*E*). The 5% small diffusive component observed at short times (Fig. 2*E Upper Inset*) also disappeared (Fig. 3*D Upper Inset*). This suggests that the small diffusive pool was not independent, but was slowly converted to an immobile membrane pool (SI). A complete suppression of recovery occurred even at very short times after drug addition (as early as 2 min, data not shown) and was reversible after washout (Fig. 3*D*), in agreement with the kinetics and reversibility reported for the effect of the drug (19).

To further confirm the central role of endocytosis in E-cadherin dynamics, we used another blocker of endocytosis, MiTMAB (21). MiTMAB inhibits the GTPase activity of dy-

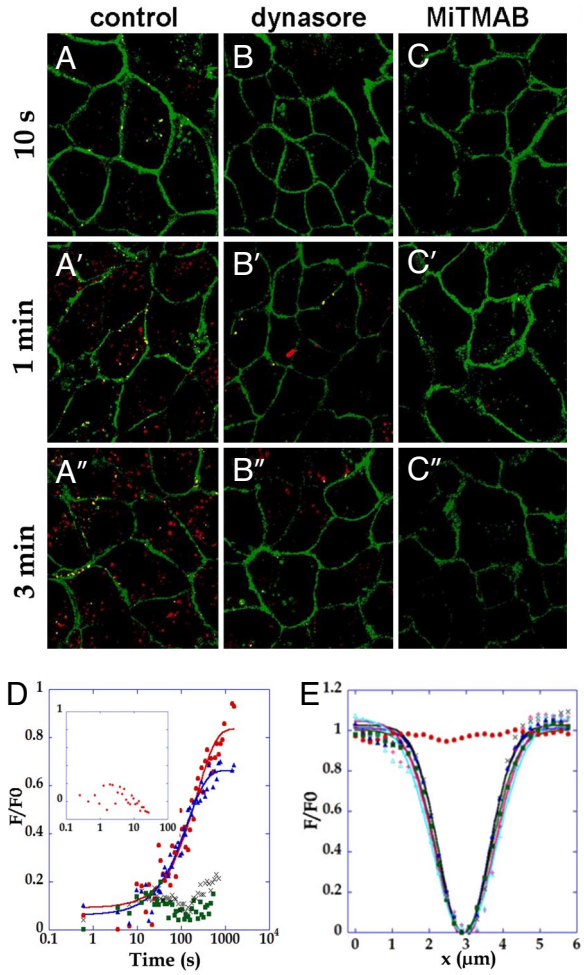

Fig. 3. E-cadherin mobility in MDCK junctions is suppressed by blocking endocytosis with dynasore or MiTMAB. (*A–C*) After treatment with control medium (*A*, *A′*, and *A″*), dynasore 60 μM (*B*, *B′*, and *B″*) or MiTMAB 30 μM (*C*, *C′*, and *C″*) MDCK E-cadherin-GFP cells were incubated with FM 4–64 5 μg/mL for the indicated times to visualize newly formed endocytosis vesicles. Merge image of the green and red staining are shown, and colocalisation appears in yellow. (*D*) Fluorescence recovery curve of E-cadherin in cells treated for 15 min with 60-μm dynasore (green) or 30 μM MiTMAB (gray) compared with cells treated with DMSO vector (red) or after washing in DMEM + vector (blue) (n = 16). (*Upper Left Inset*) Short timescale (Δt = 100 ms) mean FRAP curve after a 15-min dynasore incubation (60 μM) (n = 10). (*E*) Fluorescence profiles in cells treated 15 min with dynasore, and observed 0.6 s (blue triangle), 43 s (green square), 160 s (black x), 340 s (pink +) or 510 s (cyan triangle) after photobleaching.

namin-1 by targeting dynamin-phospholipid interactions at the membrane. MiTMAB, which is chemically unrelated to dynasore, inhibits receptor-mediated endocytosis in a range of cells (21). After 20-min treatment with 30 μM MiTMAB, the dynamics of cadherin-GFP was blocked, in a way that very much ressembles the effect of dynasore (Fig. 3*D*). Vesicle formation from the plasma membrane was also very efficiently inhibited (Fig. 3 *C–C″* and Table 1). Importantly, E-cadherin containing vesicles were formed with similar rates in wild-type and transfected MDCK cells. This is in agreement with Western blot data showing that the total amount of E-cadherin is the same in transfected and wild-type MDCK, suggesting that E-cadherin-GFP can substitute for the endogenous molecule (SI). The inhibition of E-cadherin recovery by 2 chemically distinct blockers of endocytosis, dynasore or MiTMAB, strongly supports the notion that cadherin mobility at mature *adherens* junctions in MDCK cells is mainly due to endocytosis.

E-Cadherin Dynamics in MCF7 Junctions Reflects Reaction-Limited Exchange Due to Endocytosis, with a Residence Time of 50 s. In parallel to studies with MDCK cells, a similar work was carried out with MCF7 cells to further test the role of endocytosis and comparatively evaluate the residence time of E-cadherin at the plasma membrane for cells with different adhesive properties. In MCF7 cells, E-cadherin labeling at junctions was weaker than in MDCK cells, but stronger E-cadherin vesicular staining was observed (Fig. 4*A* and SI). As for MDCK cells, the total amount of E-cadherin is the same in transfected and wild-type MCF7 cells (SI). Contrary to MDCK cells (15), E-cadherin endocytosis has been described to be mediated by a clathrin-independent pathway in isolated MCF7 cells (22). In line with these reported results we observed only partial inhibition of FRAP recovery after dynasore and MiTMAB treatments in MCF7 cells (see SI).

The analysis of fluorescence intensity profiles along junctions showed no broadening with time during fluorescence relaxation, suggesting that photobleached molecules do not diffuse in the membrane (Fig. 4 *B* and *C*). A first-order rate-limited relaxation is observed instead. As in MDCK cells, an upper bound for the contribution of a small diffusive pool to relaxation was estimated. The diffusive component represents a maximal fraction of 10% as determined from the error bars of the Gaussian width (Fig. 4*C*).

Recovery kinetics could be fitted by a single exponential with a residence time of 50 s (38–62 s) (Fig. 4*D*), but could not be fitted by a diffusion behavior. Moreover, when a broader zone was photobleached with multiple bleached points (0.5 μm to 0.8 and 1.2 μm) in the *adherens* junction plane, no significant effect was seen on the recovery kinetics (Fig. 4*D Inset*). Note that the faster E-cadherin endocytosis rate in MCF7 vs. MDCK occurs in the context of a faster endocytosis of the whole membrane, as evidenced by FM4–64 vesicle counting (see Table 1 of SI). Taken together, our results indicate the dominant contribution of a first-order reaction-limited process and support the notion that endocytosis drive E-cadherin turnover dynamics at adherens junctions.

Discussion

We show that E-cadherin dynamics in mature junctions of 2 different epithelial cell lines, MCF7 and MDCK, mainly reflects a first-order reaction exchange due to endocytosis/exocytosis processes.

The present observation that there is no significant membrane diffusion of E-cadherin in mature MDCK or MCF7 junctions is not in agreement with several previous reports showing extensive E-cadherin diffusion at the plasma membrane. This may be because these studies did not examine mature adherens junctions. Several investigations were performed in the context of isolated cell with no intercellular contacts (10, 13, 14), whereas others were focused on adherens junctions during contact initiation (8) or between moving cells (23). In these different biological situations various behaviors were reported, including simple membrane diffusion (8, 10, 13, 14), confined diffusion (10, 14), directional flow (23), or a succession of diffusion/trapping phases (13, 14). Reported diffusion coefficients (measured by FRAP or single-particle tracking) ranged from 3×10^{-3} $\mu m^2 \cdot s^{-1}$ (14) to 3–5 $\times$ 10^{-2} $\mu m^2 \cdot s^{-1}$ (8, 10, 13).

In this study, we chose the 2-photon FRAP method because it allows the vertical extent of the photobleached zone to be controlled. The FRAP experiments reported here are performed over a wide range of time-scales, from 100 ms to 1,800 s, that gives access to diffusion coefficients between 3×10^{-5} and 2 $\mu m^2 \cdot s^{-1}$. Therefore, the present data allows us to rule out, for mature junctions, (*i*) a significant contribution of free membrane diffusion in mature junctions, or (*ii*) diffusion/trapping phases as described by Iino et al. (13) and Kusumi et al. (14), who both reported an apparent diffusion of about coefficient $D = 10^{-3}$ $\mu m^2 \cdot s^{-1}$.

Table 1. Vesicles counted in MDCK cells expressing E-cadherin-GFP

	FM4–64 vesicles			Ecadh-GFP vesicles			Colocalization		
	Control	Dynasore	MiTMAB	Control	Dynasore	MiTMAB	Control	Dynasore	MiTMAB
FM4–64 10 s	20 ± 12	0.3 ± 0.3	0				Too low → not significant		
FM4–64 1 min	77 ± 14	19 ± 5	2 ± 1	20 ± 4	15 ± 3	14 ± 2	16 ± 6% *	7 ± 4% *	<1%
FM4–64 3 min	245 ± 11	65 ± 22	1 ± 0.3				43 ± 5%**	12 ± 5%**	<1%

After treatment with the indicated reagent, MDCK E-cadherin-GFP cells were incubated with FM4–64 for 10 s, 1 min, or 3 min. Stained cytsosolic vesicles were manually counted. * and ** indicate statistically significant differences ($P < 0.05$). The difference between the number of green vesicles in MDCK cells was not statistically significant. The table represents results for one representative experiment ($n = 3$–4 for each condition, $n = 10$–12 for the MDCK green labeling). Three experiments were performed with similar relative results between the conditions, and a small multiplicative factor (≤2) on the number of red vesicles corresponding to slight variations in FM4–64 labeling procedure and conservation between experiments.

In contrast to mature junctions, diffusion was found to dominate fluorescence relaxation in dissociating junctions, with a diffusion coefficient $D = 0.0025\ \mu m^2 \cdot s^{-1}$. This apparent diffusion coefficient may correspond to alternating diffusive and binding phases (see SI). This striking difference between nonmature and mature contacts is in agreement with FRAP results established using the same MDCK cells during contact maturation (8). The free diffusing fraction detected in immature junctions is drastically diminished in mature junctions, with a 80–90% fraction of molecules that do not significantly move over a 6-min relaxation period (8, 24). In our experiments, longer observation times (20 min) clearly indicate that this fraction recovers by endocytosis. Precise relaxation measurement over longer observation times, thanks to fast 3D videomicroscopy and tracking allowing to compensate for the movement of junctions, represents a significant improvement compared with our studies in refs. 16 and 17.

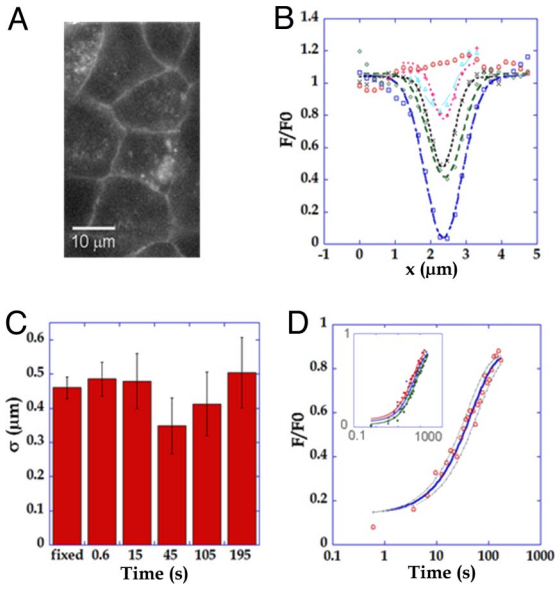

Fig. 4. Two-photon FRAP experiments at mature *adherens* junctions of MCF7-E-cadherin-GFP cells. (*A*) Typical image of MCF7 cells stably expressing E-cadhering GFP. (*B*) Profile analysis of fluorescence recovery. 17 fluorescence profile mean curves before bleaching (red circle) and at 0.6 s (blue square), 15 s (green diamond), 45 s (black x), 105 s (pink +), and 195 s (cyan triangle) after photobleaching are shown. All postbleach curves are fit by Gaussian models (dashed lines). (*C*) The widths of the gaussians at different times after photobleaching are compared with the reference width after photobleaching in fixed cells. The error bars are larger than for MDCK cells (Fig. 2) due to a decreased signal/noise ratio in MCF7 cells. (*D*) The recovery curve (red circle, $n = 25$) is well fit by a first-order exchange model with $k_{off} = 0.0021 \pm 0.05\ s^{-1}$. (*Upper Left Inset*) Linear time axis representation. Photobleaching spots of 0.5 ($n = 25$, red circle), 0.8 ($n = 16$, blue triangle) and 1.2 ($n = 15$, green square) μm width along the junction axis are fitted by first-order exchange with similar coefficients: $k_{off} = 0.021 \pm 0.005$, 0.018 ± 0.005 and $0.015 \pm 0.005\ s^{-1}$ respectively.

In mature junctions, we found that cadherin dynamics is dominated by endocytosis. A minor pool of rapidly moving E-cadherin (5%) was also detected, which likely corresponds to cadherins that freely diffuse before their irreversible engagement ($k_{eng} > 20k_{dis}$) (see SI). Indeed, it has been observed that before engagement N-cadherin similarly undergoes first free diffusion during the first seconds of the contacts before the onset of *trans* interactions (25).

Observations reported in the litterature indicate that endocytosis would concern only a limited pool (10–15%) of E-cadherin molecules (15) (26), and cell-free assay data suggest that cadherins do not undergo clathrin-dependant endocytosis when interacting in *trans* (27). In contrast, our results indicate that all E-cadherin molecules, interacting both in *trans* and *cis*, have the same fast recycling kinetics, in agreement with the observed short lifetime of *trans* dimers (11). Interestingly, endocytosis rate depends on the cell type, and is much faster than the half-life of E-cadherin [≈20 h in A431 cells (28)].

The prevalent view states that, after engagement, cadherins detach and diffuse freely in the membrane before being endocytosed. Another recent study indicates that in remodelling epithelia during *Drosophila* development, clusters of E-cadherin and associated junction proteins laterally move in a constrained fashion limited by actin tethering (29). Note that in that model, free cadherins do not diffuse inside or out of these highly adhesive structures. The main finding of our article is that cadherin removal from the mature junctions between mammalian epithelial cells (in which we cannot detect such clusters of adhesion proteins) does not involve a significant free diffusion phase and that it requires endocytosis. This prompts the hypothesis that the endocytosis machinery directly extracts cadherins from adhesive bonds. The notion that endocytosis is the driving force for the disassembly of cadherin dimer has been already proposed by Troyanovsky et al. (11), using a biochemical approach.

The hypothesis that cadherins are mostly irreversibly engaged and then extracted from *cis* or *trans* bonds directly by endocytosis machinery fits with the observation that the strength of the acto-myosin cortex interferes with the endocytosis efficiency (30). In that context, the mechanical forces involved in intercellular adhesion must be considered (31), and a difficult problem is raised to know the forces associated with cadherin extraction and endocytosis. Moreover, if endocytosis is assumed to perform a mechanical work, its biochemistry is likely to be mechanosensitive, and this could play a role for controlling intercellular adhesion forces, ultimately providing a possibility for the dynamic stabilization of epithelia.

Materials and Methods

Cell Culture and Pharmacological Treatments. Cells were grown in DMEM supplemented with 10% FCS and 0.4 mg/mL geneticin (Invitrogen). MDCK cells

expressing stably canine E-cadherin-GFP were a gift from W. J. Nelson (Stanford University, Stanford, CA) (8). The plasmid coding for human E-cadherin-GFP was a gift from A. Bershadsky (Weizmann Institute, Rehovot, Israel). From MCF7 cells, stable E-cadherin-GFP transfectants (Lipofectamine 2000; Invitrogen) were selected with geneticin, and the clone showing the brightest fluorescence at junctions was studied. Endocytosis was blocked with 60 μM dynasore (*N*′-[(1E)-(3,4-dihydroxyphenyl)methylene]-3-hydroxy-2-naphtohydrazide; ArONIS) (19) or MiTMAB (myristyl trimethyl ammonium bromide; Calbiochem) (21) in FCS-free medium, using incubation times ranging from 2 to 30 min.

Visualization of Newly Formed Endocytosis Vesicles. Upon treatment with specified reagents, MDCK E-cadherin-GFP cells were incubated with FM4–64FX (Invitrogen) 5 μg/mL for various times, rinsed 3 times in cold PBS and fixed with 4% paraformaldehyde/0.25% glutaraldehyde in PBS. They were then observed by confocal microscopy (Leica SP2 AOBS). To count newly formed vesicles, 8 bits images were first binarized with a common threshold, bright single-pixels spots were filtered out, and red and green images were merged. Vesicles were manually counted to select points in the cytosol only. For the sake of the presentation, and to make yellow points visible despite reduced image sizes, yellow points have been dilated. Original images are shown in the SI.

Two-Photon FRAP with Fast 3D Videomicroscopy. Cells were observed 3 days after seeding on glass coverslips, and ≈12–24 h after confluency, in DMEM–FCS supplemented with 10 mM Hepes, in a 37 °C observation chamber (POC-mini-chamber-system, Tempcontrol 37–2 Digital PeCon), on an IX71 inverted microscope (Olympus) with a high numerical aperture objective (63× oil-immersion, NA = 1.25, PlanNeofluar, Zeiss).

Two-photon photobleaching was performed with a femto-second laser tuned at 878 nm, pumped by a 10W CW 532 nm laser (Mira 900 and Verdi; Coherent). The position of the beam was controlled by VM500 galvanometric mirrors (GSI Lumonics) and the photobleaching duration by a shutter LS200 (NnmLaser), driven by MetaMorph. The measured excitation Point-Spread Function (PSF) is an ellipsoid with a 0.5-μm diameter in the focal plane and a 1.5-μm extension along the optical axis. Fluorescence recovery was spatially resolved under 1-photon excitation by fast 3D wide field videomicroscopy, using a DG-4 monochromator set at 480 nm (Sutter), a Coolsnap HQ CCD camera (Roper Scientific), and a PiFoc piezo-driven objective actuator (Physik Instrumente). FRAP experiments were performed as follows. One point in a junction was photobleached for 200 ms with a 30 mW average power excitation intensity as measured at the objective back pupil. Stacks of 10–20 images with a 0.3-μm vertical spacing were acquired before and after photobleaching with a time interval Δt ranging from 100 ms to 30 s. FRAP movies are provided in the SI.

Analysis and Interpretation of the FRAP Data. Image stack analysis was performed using a home-made Matlab program (Mathworks) (code available upon request). Line intensity profiles were manually followed as a function of time with the possibility of correcting for possible transversal motions. These profiles were low-pass filtered over the waist of the PSF. Unwanted photobleaching during the recovery (at least 5–10% in 30 s as assessed on fixed cells) was corrected for by normalizing intensity histograms at each time point (see SI). Fluorescence relaxation was analyzed either spatially or at a single point. The curves were normalized in such a way that 100% corresponded to the prebleach intensity and the 0% level corresponded to the level reached upon maximal bleaching depth, i.e., reached under equivalent conditions with paraformaldehyde-fixed GFP-expressing cells. FRAP data were analyzed using a diffusion- or reaction-limited model (see *Results* and SI).

ACKNOWLEDGMENTS. We thank Alexander Bershadsky for the gift of E-cadherin plasmid and fruitful discussions; Dr W. J. Nelson for kindly providing MDCK-cadherin-GFP cells; Christophe Lamaze for seminal suggestions; and Monique Arpin, Ellen Batchelder, Sylvie Dufour, Sandrine Etienne-Manneville, and François Waharte for helpful discussions and critical reading of the manuscript. This work was supported by grants from the Institut Curie, the Canceropole Ile-de-France, the Fondation pour la Recherche Médicale, and the Centre National de la Recherche Scientifique (to the Amblard's group). S.d.B. holds a PhD fellowship from Ministere de l'Education Nationale de la Recherche et de Technologie.

1. Gumbiner BM (2005) Regulation of cadherin-mediated adhesion in morphogenesis. *Nat Rev Mol Cell Biol* 6:622–634.
2. Takeichi M (1995) Morphogenetic roles of classic cadherins. *Curr Opin Cell Biol* 7:619–627.
3. Yap AS (1998) The morphogenetic role of cadherin cell adhesion molecules in human cancer: A thematic review. *Cancer Invest* 16:252–261.
4. Drees F, et al. (2005) Alpha-catenin is a molecular switch that binds E-cadherin-beta-catenin and regulates actin-filament assembly. *Cell* 123:903–915.
5. Leckband D, Sivasankar S (2000) Mechanism of homophilic cadherin adhesion. *Curr Opin Cell Biol* 12:587–592.
6. Ozawa M (2002) Lateral dimerization of the E-cadherin extracellular domain is necessary but not sufficient for adhesive activity. *J Biol Chem* 277:19600–19608.
7. Troyanovsky RB, Sokolov E, Troyanovsky SM (2003) Adhesive and lateral E-cadherin dimers are mediated by the same interface. *Mol Cell Biol* 23:7965–7972.
8. Adams CL, Chen YT, Smith SJ, Nelson WJ (1998) Mechanisms of epithelial cell–cell adhesion and cell compaction revealed by high-resolution tracking of E-cadherin-green fluorescent protein. *J Cell Biol* 142:1105–1119.
9. Klingelhofer J, Laur OY, Troyanovsky RB, Troyanovsky SM (2002) Dynamic interplay between adhesive and lateral E-cadherin dimers. *Mol Cell Biol* 22:7449–7458.
10. Sako Y, Nagafuchi A, Tsukita S, Takeichi M, Kusumi A (1998) Cytoplasmic regulation of the movement of E-cadherin on the free cell surface as studied by optical tweezers and single particle tracking: Corralling and tethering by the membrane skeleton. *J Cell Biol* 140:1227–1240.
11. Troyanovsky RB, Sokolov EP, Troyanovsky SM (2006) Endocytosis of cadherin from intracellular junctions is the driving force for cadherin adhesive dimer disassembly. *Mol Biol Cell* 17:3484–3493.
12. Bryant DM, Stow JL (2004) The ins and outs of E-cadherin trafficking. *Trends Cell Biol* 14:427–434.
13. Iino R, Koyama I, Kusumi A (2001) Single molecule imaging of green fluorescent proteins in living cells: E-cadherin forms oligomers on the free cell surface. *Biophys J* 80:2667–2677.
14. Kusumi A, Sako Y, Yamamoto M (1993) Confined lateral diffusion of membrane receptors as studied by single particle tracking (nanovid microscopy). Effects of calcium-induced differentiation in cultured epithelial cells. *Biophys J* 65:2021–2040.
15. Le TL, Yap AS, Stow JL (1999) Recycling of E-cadherin: A potential mechanism for regulating cadherin dynamics. *J Cell Biol* 146:219–232.
16. Coscoy S, et al. (2002) Molecular analysis of microscopic ezrin dynamics by two-photon FRAP. *Proc Natl Acad Sci USA* 99:12813–12818.
17. Waharte F, Brown CM, Coscoy S, Coudrier E, Amblard F (2005) A two-photon FRAP analysis of the cytoskeleton dynamics in the microvilli of intestinal cells. *Biophys J* 88:1467–1478.
18. Sprague BL, Pego RL, Stavreva DA, McNally JG (2004) Analysis of binding reactions by fluorescence recovery after photobleaching. *Biophys J* 86:3473–3495.
19. Macia E, et al. (2006) Dynasore, a cell-permeable inhibitor of dynamin. *Dev Cell* 10:839–850.
20. Newton AJ, Kirchhausen T, Murthy VN (2006) Inhibition of dynamin completely blocks compensatory synaptic vesicle endocytosis. *Proc Natl Acad Sci USA* 103:17955–17960.
21. Quan A, et al. (2007) Myristyl trimethyl ammonium bromide and octadecyl trimethyl ammonium bromide are surface-active small molecule dynamin inhibitors that block endocytosis mediated by dynamin I or dynamin II. *Mol Pharmacol* 72:1425–1439.
22. Paterson AD, Parton RG, Ferguson C, Stow JL, Yap AS (2003) Characterization of E-cadherin endocytosis in isolated MCF-7 and chinese hamster ovary cells: The initial fate of unbound E-cadherin. *J Biol Chem* 278:21050–21057.
23. Kametani Y, Takeichi, M (2007) Basal-to-apical cadherin flow at cell junctions. *Nat Cell Biol* 9:92–98.
24. Yamada S, Pokutta S, Drees F, Weis WI, Nelson WJ (2005) Deconstructing the cadherin-catenin-actin complex. *Cell* 123:889–901.
25. Lambert M, Choquet D, Mege RM (2002) Dynamics of ligand-induced, Rac1-dependent anchoring of cadherins to the actin cytoskeleton. *J Cell Biol* 157:469–479.
26. Miyashita Y, Ozawa M (2007) Increased internalization of p120-uncoupled E-cadherin and a requirement for a dileucine motif in the cytoplasmic domain for endocytosis of the protein. *J Biol Chem* 282:11540–11548.
27. Izumi G, et al. (2004) Endocytosis of E-cadherin regulated by Rac and Cdc42 small G proteins through IQGAP1 and actin filaments. *J Cell Biol* 166:237–248.
28. Davis MA, Ireton RC, Reynolds AB (2003) A core function for p120-catenin in cadherin turnover. *J Cell Biol* 163:525–534.
29. Cavey M, Rauzi M, Lenne PF, Lecuit T (2008) A two-tiered mechanism for stabilization and immobilization of E-cadherin. *Nature* 453:751–756.
30. Carramusa L, Ballestrem C, Zilberman Y, Bershadsky AD (2007) Mammalian diaphanous-related formin Dia1 controls the organization of E-cadherin-mediated cell–cell junctions. *J Cell Sci* 120:3870–3882.
31. Bell GI (1978) Models for the specific adhesion of cells to cells. *Science* 200:618–627.